npj | Quantum Materials

ARTICLE **OPEN**

Anomalous orbital structure in a spinel–perovskite interface

Yanwei Cao[1], Xiaoran Liu[1], Padraic Shafer[2], Srimanta Middey[1], Derek Meyers[1,3], Mikhail Kareev[1], Zhicheng Zhong[4,5], Jong-Woo Kim[6], Philip J Ryan[6], Elke Arenholz[2] and Jak Chakhalian[1,7]

In all archetypical reported (001)-oriented perovskite heterostructures, it has been deduced that the preferential occupation of two-dimensional electron gases is in-plane d_{xy} state. In sharp contrast to this, the investigated electronic structure of a spinel-perovskite heterostructure γ-Al_2O_3/$SrTiO_3$ by resonant soft X-ray linear dichroism, demonstrates that the preferential occupation is in out-of-plane d_{xz}/d_{yz} states for interfacial electrons. Moreover, the impact of strain further corroborates that this anomalous orbital structure can be linked to the altered crystal field at the interface and symmetry breaking of the interfacial structural units. Our findings provide another interesting route to engineer emergent quantum states with deterministic orbital symmetry.

npj Quantum Materials (2016) **1**, 16009; doi:10.1038/npjquantmats.2016.9;

INTRODUCTION

Identifying the orbital symmetry of electrons near the Fermi edge is fundamentally important for understanding phase components of the order parameter,[1–5] the coexistence of superconductivity and ferromagnetism,[6–9] and the high mobility of interfacial conduction electrons.[10–12] For example, at titanates based perovskite–perovskite interfaces, the preferential occupation of an in-plane d_{xy} state by conduction electrons defines the isotropy of the Fermi surface[13–25] of the two-dimensional (2D) electron gas. Theoretical calculations have predicted the possibility of out-of-plane d_{xz}/d_{yz} orbital symmetry of conduction carriers in titanates[25] that can lead to an unusual one-dimensional (1D) electronic structure marked by either two orthogonal 1D bands[26–28] with degenerate d_{xz}/d_{yz} orbitals or a single 1D band with non-degenerate d_{xz} and d_{yz} orbitals.[12,19,29] Despite extensive experimental search thus far, however, this anomalous orbital configuration has not been observed at (001)-oriented interfaces.[18]

Very recently with the observation of interface enhanced high-temperature superconductivity (60–100 K)[30,31] and high-mobility conduction electrons (~1.4×10^5 $cm^2\,V^{-1}\,s^{-1}$)[10] in $SrTiO_3$ (STO)-based interfaces, probing the interactions between charge, spin, orbital, and structural degrees of freedom at the interfaces became fundamentally important to understand interface enhanced emergent electronic states. Specifically, the orbital symmetry of conduction carriers is primarily linked to the symmetry of the superconducting gap[4] and the mobility of electrons.[10–12] To this end, the orbital configuration, responsible for the high mobility of electrons in a spinel–perovskite interface (for example γ-Al_2O_3/$SrTiO_3$, AlO/STO)[10,11,32] is still an open question. From the experimental point of view, surface sensitive angle-resolved photoemission spectroscopy with polarized photons is a suitable probe of symmetry of the surface electronic structure,[19] but it has limited applicability for the electronically active buried interfaces. In contrast to angle-resolved photoemission spectroscopy, interface sensitive linearly polarized X-ray absorption spectroscopy (XAS) has proven to be a powerful tool to resolve the orbital symmetry.[6,9,13–18,33,34]

In this work, using the AlO/STO heterostructure as a model system, we report on unique orbital symmetry and orbital occupancy, which is reversed compared with other well-known 2D electron gases based on perovskite titanates. Resonant soft X-ray linear dichroism (XLD) studies combined with direct current transport measurements have confirmed the orbital symmetry inversion driven by the altered crystal field at the interface and symmetry breaking of the TiO_6 octahedral units.

RESULTS

High-quality AlO/STO heterostructures were synthesized by pulsed laser deposition (see Supplementary Figure 1 and Materials and Methods for details). With its spinel structure, bulk γ-Al_2O_3 is cubic (space group $Fd\bar{3}m$) with a lattice parameter $a=7.911$ Å,[35,36] which is close to twice of the lattice parameter of bulk $SrTiO_3$ $a=3.905$ Å. It is interesting to note that γ-Al_2O_3 is generally regarded as a defect spinel $Al_{8/3}O_4$ (32 oxygen ions, 64/3 Al cations, and 8/3 vacancies for one unit cell γ-Al_2O_3), which has the analogous structure to the conventional spinel $MgAl_2O_4$;[36] owing to the Al vacancies, polar mismatch may be present at AlO/STO interfaces.[37] The conductivity of the AlO/STO heterostructures used in this work is in good agreement with the previous reports,[10,32,37–39] as shown in Supplementary Figure 2.

Figure 1 shows the spectra obtained by linearly polarized X-rays at the Ti $L_{2,3}$-edge of AlO/STO heterostructures. The features of XAS spectra is the result of transitions from core levels to unoccupied valence states (e.g., $2p\rightarrow3d$ for Ti L-edge). Owing to the crystal field, the Ti 3*d* state splits into t_{2g} (d_{xy}, d_{xz}, and d_{yz}) and e_g ($d_{x^2-y^2}$ and $d_{3z^2-r^2}$) subbands with a crystal field gap as large as ~2 eV in the octahedral symmetry.[9,13–18] In addition, the strong spin–orbit interaction induces the splitting of the Ti 2*p* core level into $2p_{1/2}$ and $2p_{3/2}$ states. Therefore, four main features are commonly observed in Ti L-edge XAS spectra

---

[1]Department of Physics, University of Arkansas, Fayetteville, AR, USA; [2]Advanced Light Source, Lawrence Berkeley National Laboratory, Berkeley, CA, USA; [3]Department of Condensed Matter Physics and Materials Science, Brookhaven National Laboratory, Upton, NY, USA; [4]Institut für Theoretische Physik und Astrophysik, Universität Würzburg, Am Hubland, Germany; [5]Max-Planck-Institut für Festkörperforschung, Stuttgart, Germany; [6]Advanced Photon Source, Argonne National Laboratory, Argonne, IL, USA and [7]Department of Physics and Astronomy, Rutgers University, Piscataway, NJ, USA.
Correspondence: Y Cao (yc003@uark.edu)

Received 13 June 2016; revised 6 July 2016; accepted 7 July 2016

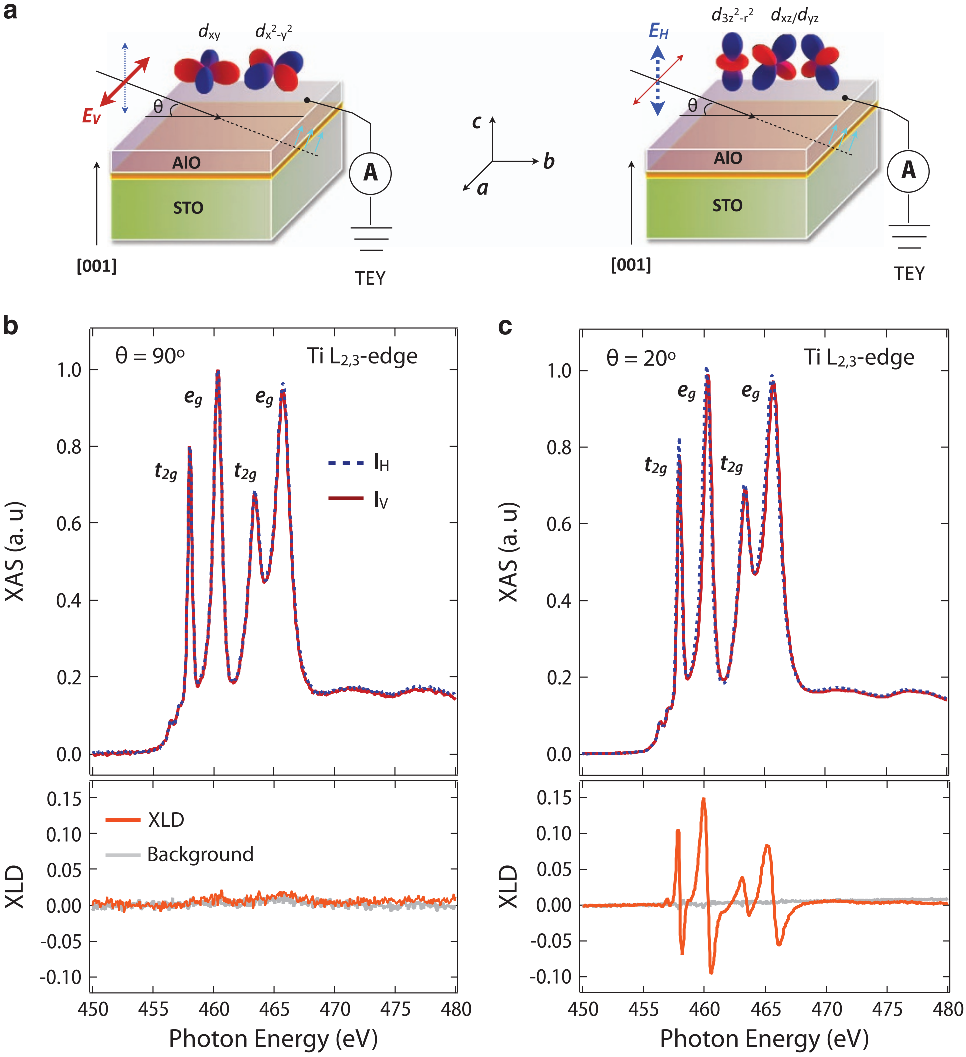

Figure 1. Linearly polarized XAS of AlO/STO at Ti $L_{2,3}$-edge. (**a**) Schematic of experimental setup. In-plane (I_V, $E_V||ab$ and E is the linear polarization vector of the photon) and out-of-plane (I_H, θ is the angle between E_H and c) linearly polarized X-ray were used to measure XAS of AlO/STO (thickness of AlO film is ~5.5 unit cells or 4.35 nm) at Ti $L_{2,3}$-edge with total electron yield (TEY, interface sensitive) detection mode at room temperature. The contribution of linearly polarized XAS signal at Ti $L_{2,3}$-edge for t_{2g} (or e_g) band mainly arises from the unoccupied Ti d_{xy}(or $d_{x^2-y^2}$) states by in-plane I_V and d_{xz}/d_{yz} (or $d_{3z^2-r^2}$) states by out-of-plane I_H. Here the signal of XLD is defined as $\text{XLD} = (I_H - I_V)$. (**b**) XAS at Ti $L_{2,3}$-edge with normal incident angle $\theta = 90°$. Both $E_V||ab$ and $E_H||ab$. (**c**) XAS at Ti $L_{2,3}$-edge with grazing incident angle $\theta = 20°$. As seen in **a**, $E_V||ab$, whereas $E_H||c$. All collected spectra are repeated more than six times.

(Figure 1b,c; Supplementary Figure 3). With lower crystal symmetry (e.g., tetragonal or orthorhombic symmetry as compared with cubic symmetry),[19] the degeneracy of t_{2g} and e_g states can be further lifted, leading to an in-plane d_{xy} subband with possibly lower energy than the out-of-plane d_{xz}/d_{yz} subband and available as the lowest energy state at the interface.[9,13–17] To investigate the orbital configuration, XAS with linearly polarized X-rays, used in this work, has been proven to be one of the most powerful available probes applied to various interfaces.[9,13–18] The utility of the probe stems from the strong dependence of absorption on the direction of the photon polarization vector (E) with respect to the crystal lattice axis (Figure 1a); Thus, excited by linearly polarized X-rays, electronic transitions from Ti core levels to the unoccupied d orbital bands contains important information about the orbital symmetry of those states. In general, when the linear X-ray polarization is oriented along the direction of unoccupied orbital lobes, the contribution of these orbitals to the XAS signal is largest.[6,33] Therefore, the X-ray absorption at the Ti $L_{2,3}$-edge for $E||ab$ and $E||c$ arises mainly from the unoccupied in-plane Ti $d_{xy}/d_{x^2-y^2}$ (I_V) and out-of-plane $d_{xz}/d_{yz}/d_{3z^2-r^2}$ (I_H) states, respectively. In general, the orbital character of a subband can be determined from the sign of XLD ~ (I_H–I_V).

For precise determination of orbital polarization the knowledge of background can be important. To confirm the low background noise level of XLD and the absence of artifacts, a normal incidence geometry ($\theta = 90°$, Figure 1b) was utilized. In this geometry, both E_H and E_V are parallel to the interfacial plane and the intensities of linearly polarized XAS should be practically identical for both X-ray polarizations (i.e., (I_H–I_V) ~ 0). As seen in Figure 1b, no significant XLD signal at Ti $L_{2,3}$-edge is observed in agreement with the expectation.[17] With the sample set at $\theta = 20°$, a strong XLD signal appears (~15% of XAS; Figure 1c) indicating the splitting of e_g and t_{2g} subbands with the lineshape that agrees well with the previous measurements and calculations.[9,13–18]

However, as seen in Figure 2, the XLD spectra for our AlO/STO system is atypical and has the reverse XLD lineshape compared with the results reported for prototypical 2D electron gases at titanate interfaces (e.g., $LaAlO_3/SrTiO_3$ (LAO/STO) and $LaTiO_3/SrTiO_3$ (LTO/STO)).[9,14–17] Specifically, for the Ti t_{2g} state of the perovsite–perovskite interfaces the negative sign of the first main

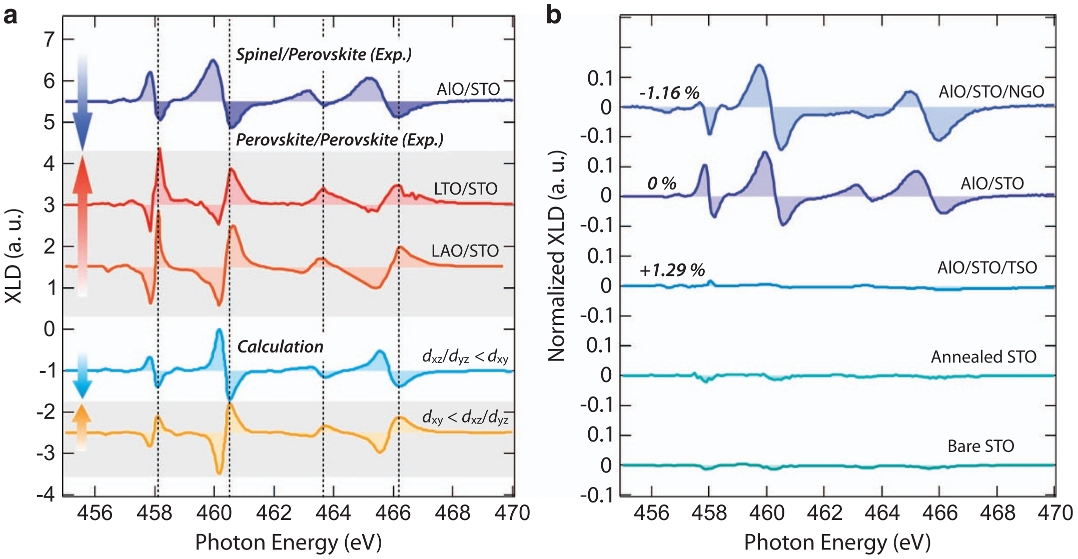

Figure 2. Symmetry inversion of XLD spectra in titanate interfaces. (**a**) The perovskite-perovskite interfaces (i.e., $LaAlO_3/SrTiO_3$ and $LaTiO_3/SrTiO_3$, red arrow) show negative sign for the first feature (at ~457.85 eV), whereas spinel-perovskite heterostructure (AlO/STO, blue arrow) displays positive sign indicating d_{xz}/d_{yz} is the preferential state of interfacial electrons for the later structure. The spectra of $LaAlO_3/SrTiO_3$ was adapted with permission from reference 16. Theoretically, to show the reversed lineshape of XLD for different orbital configurations, the calculation data were adapted with permission from reference 17. (**b**) Strain effects for AlO/STO/NGO and AlO/STO/TSO to XLD signal (compressive strain ~ −1.16 % on $NdGaO_3$ (NGO) and tensile strain ~ +1.29 % on $TbScO_3$ (TSO) substrates, respectively; thickness of STO layer is ~10 unit cells or 3.9 nm) and effects of oxygen vacancies in annealed STO single crystal to XLD signal. Comparing with the contributions from oxygen vacancies (annealed STO substrate) and bare STO substrate itself, the XLD signal at AlO/STO is robust. (Copyrighted by the American Physical Society).

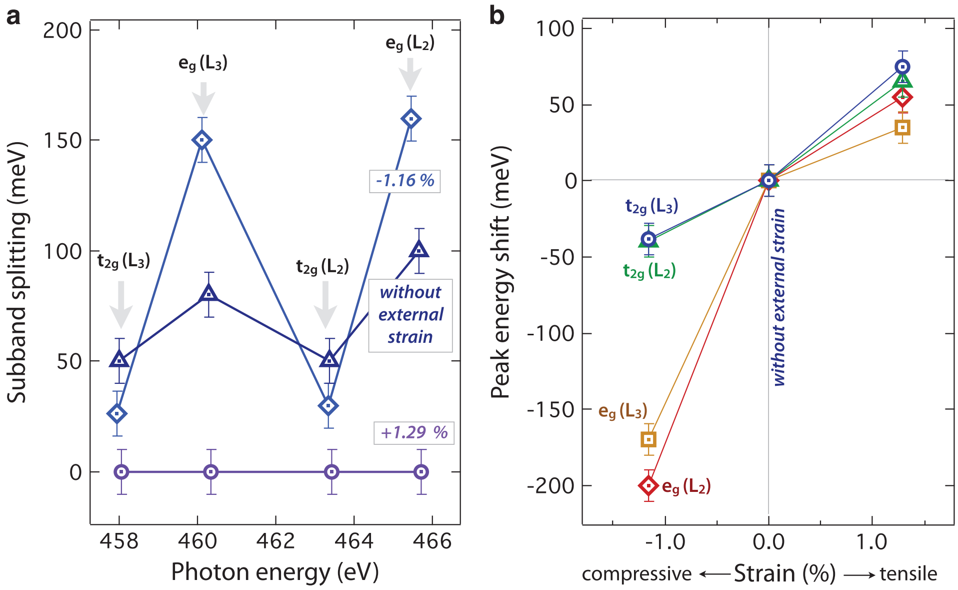

Figure 3. Strain effects of Ti 3*d* subband splitting and peak energy shift. (**a**) Subband splitting of Ti 3*d* state at AlO/STO interfaces under compressive strain ~ −1.16 % (by $NdGaO_3$ substrate, NGO), without external strain, and tensile strain ~ +1.29 % (by $TbScO_3$ substrate, TSO). (**b**) Relative peak energy shift (with unpolarized X-rays) of Ti $L_{2,3}$-band in AlO/STO interfaces under compressive strain ~ −1.16 % (negative energy direction) and tensile strain ~ +1.29 % (positive energy direction).

XLD feature implies that the d_{xy} subband is the lowest energy state in agreement with reported results.[9,13–17] In sharp contrast to this, for AlO/STO, the sign of XLD is reversed (see blue and red arrows in Figure 2a), i.e., the first feature at ~457.85 eV has a positive sign, whereas the second feature at ~458.15 eV is negative, immediately implying that d_{xz}/d_{yz} orbitals are the first available states for interfacial electrons. Therefore, the relative energy position of Ti 3*d* subbands is unusual $d_{xz}/d_{yz} < d_{xy} < d_{3z^2-r^2} < d_{x^2-y^2}$. In order to understand this anomalous behavior, epitaxial strain was induced by utilizing a large mismatch between the substrates and film (i.e., $NdGaO_3$ (NGO) substrate for compressive strain ~ −1.16 % and $TbScO_3$ (TSO) substrate for tensile strain ~ +1.29 %). As shown in Figure 2b, for the AlO/STO heterostructure on NGO (compressive strain) the lineshape of XLD is similar to that observed for AlO/STO except that the very first feature (at ~ 457.85 eV) is suppressed. However,

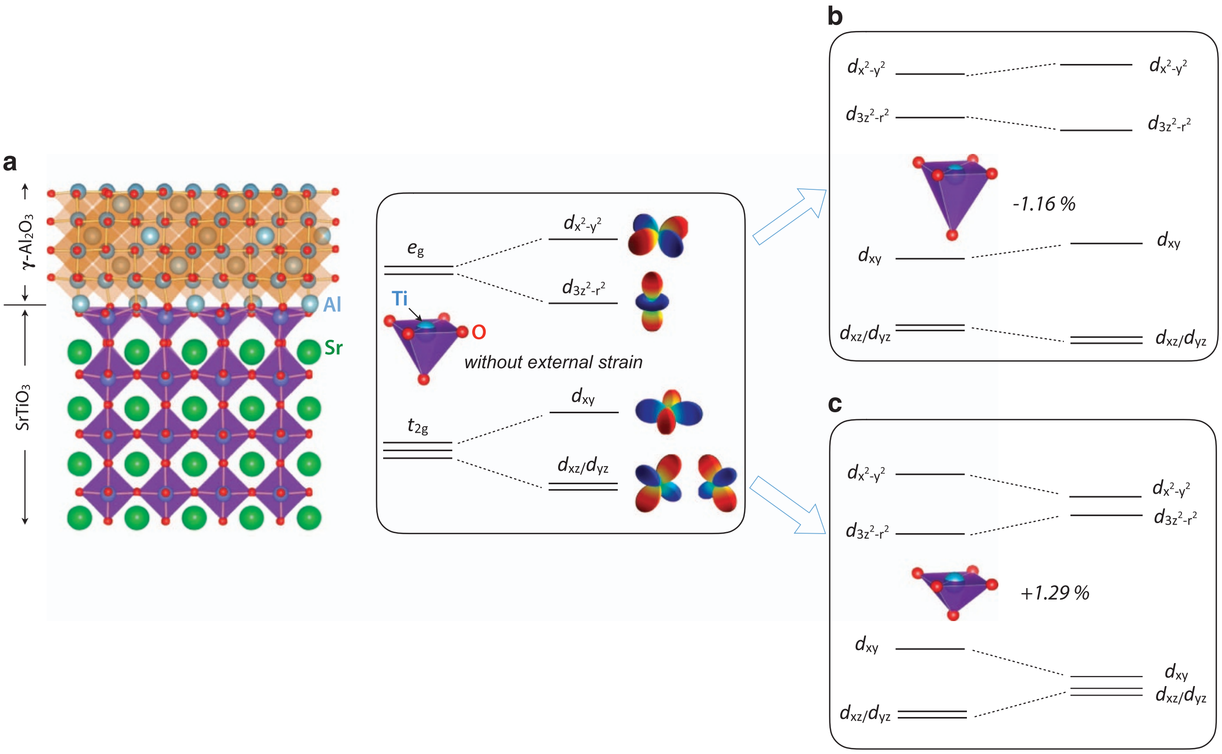

Figure 4. Strain effect of crystal field and orbital configuration for AlO/STO interface. (**a**) Schematic interfacial structure and subband splitting without external strain. (**b**) Compressive strain (~ −1.16 % by NGO substrate). (**c**) Tensile strain (~ +1.29 % by TSO substrate).

for tensile strain on TSO, surprisingly almost all the spectral features are killed and no significant XLD signal is observed.

Next, we quantify the strain effect on the splitting and peak energy shift (Figure 3). Generally, the size of the band splitting can be estimated from the peak energy difference of XAS obtained with linear polarized X-rays. First, we analyze the splitting of e_g and t_{2g} subbands at the AlO/STO interface. As shown in Figure 3a and Supplementary Figure 4, a direct comparison of the energy position for XAS with in-plane (I_V) and out-of-plane (I_H) orientation of the X-ray polarization reveal that the most pronounced XAS feature for I_H is lower in energy than the I_V absorption. For AlO/STO without external strain, it yields t_{2g} (L_3) band splitting $\Delta t_{2g} \sim 50$ meV and the $e_g(L_3)$ band splitting $\Delta e_g \sim 80$ meV. Unexpectedly, as shown in Figure 3a, under tensile strain (~ +1.29 %, on TSO substrate) the splitting of both t_{2g} and e_g bands is suppressed and practically vanished while the splitting is enhanced under compressive strain (~ −1.16 %, NGO substrate). Compared to the band splitting of AlO/STO without external strain, the e_g (L_3) band splitting Δe_g under compressive strain (~ −1.16 %) increases from ~ 80 to 150 meV, whereas the t_{2g} (L_3) band splitting $\Delta t_{2g} \sim 30$ meV is only weakly decreased. Besides the subband splitting, strain also alters the peak energy position (Figure 3b). Specifically, for tensile strain though the splitting is strongly suppressed (Figure 3a; Supplementary Figure 4) the peak energy moves to the positive direction i.e., higher photon energies by ~ +75 meV for t_{2g} (L_3) and +35 meV for e_g (L_3), respectively. On the other hand, as shown in Figure 3b, under compressive strain with enhanced band splitting, the four main peaks of Ti XAS at $L_{2,3}$-edge shift towards negative direction by about − 38 meV for t_{2g} (L_3) and − 170 meV for e_g (L_3), respectively.

DISCUSSION

Next, we discuss the atomic structure of AlO/STO interfaces as a key factor to produce the inverse orbital symmetry. As schematically shown in Supplementary Figure 5, based on the interfacial atomic structure data,[32,39] for the case of γ-Al_2O_3 spinel and in contrast to the previously reported perovskite–perovskite interfaces, the apical oxygen of Ti–O octahedra is not stable in a spinel–perovskite heterostructure. Thus, at the AlO/STO interface a unique Ti–O pyramid coordination is formed; in this distorted pyramid-like structure, d_{xz}/d_{yz} subband becomes the preferable state for the interfacial electrons (Supplementary Figure 5b,c). More importantly, the degenerate d_{xz}/d_{yz} subband can be further split owing to the cooperative efefct of spin–orbit coupling and crystal-field distortion, yielding an energy separation as large as 60–100 meV.[12,19,29] Therefore, in contrast with all reported data on the (001)-oriented perovskite interfaces with in-plane d_{xy} subband as the lowest energy state, the d_{xz} or d_{yz} subband becomes the lowest energy state for the case of spinel–perovskite heterojunction. As the consequence of the d_{xz} or d_{yz} orbital character of mobile electrons amplified by the spatial confinement along z,[40,41] and regardless of which d_{xz} or d_{yz} is the preferred state, the forbidden electron hopping along the y (for d_{xz}) or x (for d_{yz}) direction may result in the emergence of the extremely anisotropic '1D' electron gas (Supplementary Figure 5c).

Furthermore, to understand the impact of epitaxial strain on the XLD signals, we propose a simple model shown in Figure 4. As seen, under compressive strain (~ −1.16%) the contraction of the in-plane four oxygens together with the elongation of the apical oxygen ion increases the energy of the in-plane $d_{x^2-y^2}$ and d_{xy} orbitals, whereas the energy decreases for out-of-plane $d_{3z^2-r^2}$ and d_{xz}/d_{yz} orbitals.[42] As the result, the energy splitting Δe_g between $d_{x^2-y^2}$ and $d_{3z^2-r^2}$ orbitals, as well as the splitting Δt_{2g} between d_{xy} and d_{xz}/d_{yz} orbitals of Ti ions is increased. This model agrees well with the experimental observation that both Δe_g and Δt_{2g} under compressive strain are increased. On the other hand, under tensile strain, the elongation of the in-plane four oxygen ions and the contraction of the apical oxygen ion pulls the Ti ion inside the pyramid,[42] leading to the reversed effect on the Ti 3d orbital sequence. Therefore, the energy splitting within both e_g and t_{2g}

bands is expected to decrease; the corresponding XLD signal will be significantly suppressed due to the strain induced degeneracy.

In conclusion, we have demonstrated that in the *spinel-perovskite* heterostructure—AlO/STO the out-of-plane d_{xz}/d_{yz} states are the lowest lying energy states, which is in the sharp contrast to titanate based perovskite–perovskite heterostructures where the in-plane d_{xy} state is always the ground state of the 2D conduction carriers. Moreover, the impact of strain corroborates that this unusual orbital configuration is directly linked with the altered crystal field at the interface and lattice symmetry breaking of the interfacial TiO_6 octahedra. Our findings provide another interesting route to engineer unusual quantum states with deterministic orbital symmetry beyond those attainable in all (001)-oriented perovskite heterojunctions.

MATERIALS AND METHODS

Sample synthesis and characterization

Heterostructures γ-Al_2O_3 (~4.35 nm)/$SrTiO_3$ (001), γ-Al_2O_3 (~4.35 nm)/$SrTiO_3$ (~3.9 nm)/$NdGaO_3$ (110), and γ-Al_2O_3 (~4.35 nm)/$SrTiO_3$ (~3.9 nm)/$TbScO_3$ (110) were layer-by-layer epitaxially grown with pulsed laser deposition (PLD), using a KrF excimer laser operating at $\lambda = 248$ nm and 2 Hz pulse rate with 2 J/cm^2 fluence. The layer-by-layer growth was monitored by *in-situ* reflection high-energy electron diffraction. During growth we utilized low oxygen pressure (~7.5×10^{-5} torr) and the temperature of the substrates was held at 700 °C. After growth, all samples were cooled at about 15 °C/min rate to room temperature keeping oxygen pressure constant. Annealed bulk $SrTiO_3$ was prepared in vacuum (~1×10^{-6} torr) at 750 °C for 1 h. The lattice parameters of substrates are $a = 3.905$ Å for $SrTiO_3$ (STO); $a = 5.43$ Å, $b = 5.50$ Å, $c = 7.71$ Å for $NdGaO_3$ (NGO); $a = 5.46$ Å, $b = 5.72$ Å, $c = 7.91$ Å for $TbScO_3$ (TSO). The sheet-resistances of samples were measured in van-der-Pauw geometry by Physical Properties Measurement System (Quantum Design) from 300 to 2 K. X-ray diffraction was carried out at the 6-ID-B beamline of the Advanced Photon Source at Argonne National Laboratory.

Spectroscopy

XAS/XLD (at room temperature) at Ti $L_{2,3}$-edge with total electron yield detection mode (interface sensitive) were carried out at beamline 4.0.2 of the Advanced Light Source (Lawrence Berkeley National Laboratory). In successive scans, spectra were captured with the order of polarization rotation reversed (e. g., horizontal, vertical, vertical, and horizontal) so as to eliminate systematic artifacts in the signal that drift with time. The residual artifact intensity is plotted in Figure 1 and labeled as background.

ACKNOWLEDGEMENTS

We acknowledge numerous insightful theory discussions with Daniel Khomskii. J.C. was supported by the Gordon and Betty Moore Foundation EPiQS Initiative through Grant No. GBMF4534. Y.C., S.M. and M.K. were supported by the DOD-ARO under Grant No. 0402-17291. X.L. was supported by the Department of Energy Grant No. DE-SC0012375. The Advanced Light Source is supported by the Director, Office of Science, Office of Basic Energy Sciences, of the U.S. Department of Energy under Contract No. DE-AC02-05CH11231. This research used resources of the Advanced Photon Source, a U.S. Department of Energy (DOE) Office of Science User Facility operated for the DOE Office of Science by Argonne National Laboratory under Contract No. DE-AC02-06CH11357.

CONTRIBUTIONS

Y.C. and J.C. conceived and designed the experiments. Y.C., X.L., D.M., P.S. and E.A. acquired the XAS/XLD data. Y.C., X.L., S.M. and D.M. measured the electrical transport. Y.C., X.L., S.M., D.M., J.K. and P.R. measured the X-ray diffraction. M.K. and Y.C. prepared and characterized the samples. Y.C., P.S., E.A. and J.C. analyzed the data. All authors discussed the results.

COMPETING INTERESTS

The authors declare no conflict of interest.

REFERENCES

1. Tsuel, C. C. & Kirtley, J. R. Pairing symmetry in cuprate superconductors. *Rev. Mod. Phys.* **72**, 969–1016 (2000).
2. Mackenzie, A. P. & Maeno, Y. The superconductivity of Sr_2RuO_4 and the physics of spin-triplet pairing. *Rev. Mod. Phys.* **75**, 657–712 (2003).
3. Mazin, I. I. Superconductivity gets an iron boost. *Nature* **464**, 183–186 (2010).
4. Leggett, A. J. What do we know about high T_C? *Nat. Phys.* **2**, 134–136 (2006).
5. Borisenko, S. V. *et al.* One-sign order parameter in iron based superconductor. *Symmetry* **4**, 251–264 (2012).
6. Chakhalian, J., Freeland, J. W., Millis, A. J., Panagopoulos, C. & Rondinelli, J. M. Colloquium: Emergent properties in plane view: Strong correlations at oxide interfaces. *Rev. Mod. Phys.* **86**, 1189–1202 (2014).
7. Dikin, D. A. *et al.* Coexistence of superconductivity and ferromagnetism in two dimensions. *Phys. Rev. Lett.* **107**, 056802 (2011).
8. Michaeli, K., Potter, A. C. & Lee, P. A. Superconducting and ferromagnetic phases in $SrTiO_3/LaAlO_3$ oxide interface structures: possibility of finite momentum pairing. *Phys. Rev. Lett.* **108**, 117003 (2012).
9. Lee, J. S. *et al.* Titanium d_{xy} ferromagnetism at the $LaAlO_3/SrTiO_3$ interface. *Nat. Mater.* **12**, 703–706 (2013).
10. Chen, Y. Z. *et al.* A high-mobility two-dimensional electron gas at the spinel/perovskite interface of γ-$Al_2O_3/SrTiO_3$. *Nat. Commun.* **4**, 1371 (2013).
11. Chen, Y. Z. *et al.* Room temperature formation of high-mobility two-dimensional electron gases at crystalline complex oxide interfaces. *Adv. Mater.* **26**, 1462–1467 (2014).
12. Fête, A. *et al.* Large modulation of the Shubnikov-de Haas oscillations by the Rashba interaction at the $LaAlO_3/SrTiO_3$ interface. *New. J. Phys.* **16**, 112002 (2014).
13. Cao, Y. *et al.* Magnetic interactions at the nanoscale in trilayer titanates. *Phys. Rev. Lett.* **116**, 076802 (2016).
14. Salluzzo, M. *et al.* Orbital reconstruction and the two-dimensional electron gas at the $LaAlO_3/SrTiO_3$ Interface. *Phys. Rev. Lett.* **102**, 166804 (2009).
15. Salluzzo, M. *et al.* Structural and electronic reconstructions at the $LaAlO_3/SrTiO_3$ interface. *Adv. Mater.* **25**, 2333–2338 (2013).
16. Salluzzo, M. *et al.* Origin of interface magnetism in $BiMnO_3/SrTiO_3$ and $LaAlO_3/SrTiO_3$ heterostructures. *Phys. Rev. Lett.* **111**, 087204 (2013).
17. Pesquera, D. *et al.* Two-dimensional electron gases at $LaAlO_3/SrTiO_3$ Interfaces: Orbital symmetry and hierarchy engineered by crystal orientation. *Phys. Rev. Lett.* **113**, 156802 (2014).
18. Herranz, G. *et al.* Engineering two-dimensional superconductivity and Rashba spin-orbit coupling in $LaAlO_3/SrTiO_3$ quantum wells by selective orbital occupancy. *Nat. Commun.* **6**, 6028 (2015).
19. Santander-Syro, A. F. *et al.* Two-dimensional electron gas with universal subbands at the surface of $SrTiO_3$. *Nature* **469**, 189–193 (2011).
20. Meevasana, W. *et al.* Creation and control of a two-dimensional electron liquid at the bare $SrTiO_3$ surface. *Nat. Mater.* **10**, 114–118 (2011).
21. McKeown Walker, S. *et al.* Control of a two-dimensional electron gas on $SrTiO_3$(111) by atomic oxygen. *Phys. Rev. Lett.* **113**, 177601 (2014).
22. Plumb, N. C. *et al.* Mixed dimensionality of confined conducting electrons in the surface region of $SrTiO_3$. *Phys. Rev. Lett.* **113**, 086801 (2014).
23. Chang, Y. J. *et al.* Layer-by-layer evolution of a two-dimensional electron gas near an oxide interface. *Phys. Rev. Lett.* **111**, 126401 (2013).
24. Zhong, Z., Tóth, A. & Held, K. Theory of spin-orbit coupling at $LaAlO_3/SrTiO_3$ interfaces and $SrTiO_3$ surfaces. *Phys. Rev. B* **87**, 161102(R) (2013).
25. Zhong, Z., Wissgott, P., Held, K. & Sangiovanni, G. Microscopic understanding of the orbital splitting and its tuning at oxide interfaces. *Europhys. Lett.* **99**, 37011 (2012).
26. Coey, J. M. D., Ariando & Pickett, W. E. Magnetism at the edge: New phenomena at oxide interfaces. *MRS Bull.* **38**, 1040–1047 (2013).
27. Zhou, X. J. *et al.* One-dimensional electronic structure and suppression of *d*-wave node state in $(La_{1.28}Nd_{0.6}Sr_{0.12})CuO_4$. *Science* **286**, 268–272 (1999).
28. Yoo, H. K. *et al.* Thickness-dependent electronic structure in ultrathin $LaNiO_3$ films under tensile strain. *Phys. Rev. B* **93**, 035141 (2016).
29. Zhou, K. J. *et al.* Localized and delocalized Ti 3*d* carriers in $LaAlO_3/SrTiO_3$ superlattices revealed by resonant inelastic x-ray scattering. *Phys. Rev. B* **83**, 201402 (R) (2011).
30. Wang, Q. Y. *et al.* Interface-induced high-temperature superconductivity in single unit-cell FeSe films on $SrTiO_3$. *Chin. Phys. Lett.* **29**, 037402 (2012).
31. Ge, G. F. *et al.* Superconductivity above 100 K in single-layer FeSe films on doped $SrTiO_3$. *Nat. Mater.* **14**, 285–289 (2015).
32. Kormondy, K. J. *et al.* Quasi-two-dimensional electron gas at the epitaxial alumina/$SrTiO_3$ interface: Control of oxygen vacancies. *J. Appl. Phys.* **117**, 095303 (2015).
33. Chakhalian, J. *et al.* Orbital reconstruction and covalent bonding at an oxide interface. *Science* **318**, 1114–1117 (2007).
34. Cao, Y. *et al.* Engineered Mott ground state in a $LaTiO_{3+\delta}/LaNiO_3$ heterostructure. *Nat. Commun.* **7**, 10418 (2016).

35. Zhou, R. S. & Snyder, R. L. Structures and transformation mechanisms of the η, γ and θ transition aluminas. *Acta Crystallogr.* **B47**, 617–630 (1991).
36. Jiang, K., Music, D., Sarakinos, K. & Schneider, J. M. Ab initio study of effects of substitutional additives on the phase stability of γ-alumina. *J. Phys. Condens.* **22**, 505502 (2010).
37. Schütz, P. *et al.* Band bending and alignment at the spinel/perovskite γ-Al_2O_3/$SrTiO_3$ heterointerface. *Phys. Rev. B* **91**, 165118 (2015).
38. Ngo, T. Q. *et al.* Quasi-two-dimensional electron gas at the interface of γ-Al_2O_3/$SrTiO_3$ heterostructures grown by atomic layer deposition. *J. Appl. Phys.* **118**, 115303 (2015).
39. Lu, S. *et al.* Spectrum and phase mapping across the epitaxial γ-Al_2O_3/$SrTiO_3$ interface. *Appl. Phys. Lett.* **108**, 051606 (2016).
40. Ohtomo, A., Muller, D. A., Grazul, J. L. & Hwang, H. Y. Artificial charge-modulationin atomic-scale perovskite titanate superlattices. *Nature* **419**, 378–380 (2002).
41. You, J. H. & Lee, J. H. Critical thickness for the two-dimensional electron gas in $LaTiO_3$/$SrTiO_3$. *Phys. Rev. B* **88**, 155111 (2013).
42. Khomskii, D. I. *Transition Metal Compounds*. Cambridge Univ. Press, (2014).

Supplementary Information accompanies the paper on the *npj Quantum Materials* website (http://www.nature.com/npjquantmats)